Random Field Modeling for the Prediction of Wall Thickness of Nuclear Pipes Considering Data Misalignment

Adetola Adegbola
Graduate Student, Dept. of Civil Engineering, Ryerson University, Toronto, Canada

Xian-Xun Yuan
Associate Professor, Dept. of Civil Engineering, Ryerson University, Toronto, Canada

Min Wang
Senior Analyst, CANDU Energy Inc., Mississauga, Canada

ABSTRACT: Probabilistic structural integrity assessment has been increasingly used to ensure the fitness-for-service of the major systems, structures and components (SSCs) of a nuclear power plant. The probabilistic approach requires a sophisticated mathematical model to quantify the variability and uncertainty of the degradation involved in the SSCs. This paper presents a nonhomogeneous random field modeling approach to the prediction of wall thickness of nuclear pipes due to flow-accelerated corrosion. The approach addresses two practical issues in random field-based degradation modeling. It uses a moving-window kriging technique to estimate the missing measurements involved in ultrasonic scans, and then stitch the overlapping scan patches to make a whole random field for the wall thickness. The uniform random field becomes an important input for next-step structural integrity assessment using, e.g., stochastic finite element analysis. The proposed modeling approach is illustrated by a practical example of nuclear feeder piping.

1. INTRODUCTION

As a part of the primary heat transport system (PHTS) of a CANDU reactor, feeder pipes fabricated from carbon steel in nuclear power plants experience degradation over time in form of wall thinning due to flow-accelerated corrosion (FAC). Disposition is required if the extent of piping local wall loss exceed the limits specified for the design of the piping component to ensure the continuing safe operation of the power plants. While a simplified flaw disposition would require only the minimum wall thickness at the region of interest, detailed finite element analysis (FEA) is usually preferred for the fitness for service assessment. Wall thickness profile is a key input both for the FEA modeling and to derive the pipe loads which are then fed into the FEA.

FAC is a type of steel corrosion exacerbated by coolant flow in feeder pipes at high velocities and temperatures. Factors known to affect the rate of FAC include mass transfer, coolant flow velocity, pipe material composition in terms of chromium content, stress levels such as temperature and pressure, bend angle, coolant pH and oxidizing species (Chung, 2010; Slade and Gendron, 2005). A feeder consists of a number of bends, each bend being further divided into four zones: extrados, intrados, left cheek, and right cheek (Figure 1). Yet the most severe wall thinning is often observed on the extrados of a bend, in which two thinning mechanisms present. The first one is called fabrication thinning; namely, during mechanical bending of straight new feeder pipes with uniform wall thickness, the extrados of a bend gets thinner while the intrados becomes thicker. The second wall thinning mechanism is FAC corrosion. It has been generally accepted that the greater FAC rate at extrados can be attributed to the greater turbulence at the extrados when flow of heavy

water makes turns in the feeder pipe. More recently, highly localized thinning was observed close to the grayloc weld, well away from the first bend, in a feeder removed from the Pickering station (Jin and Awad, 2011). This shows the need to develop a methodology that fully considers the overall wall thickness profiles of feeder pipes, instead of just focusing attention on what happens at bends only.

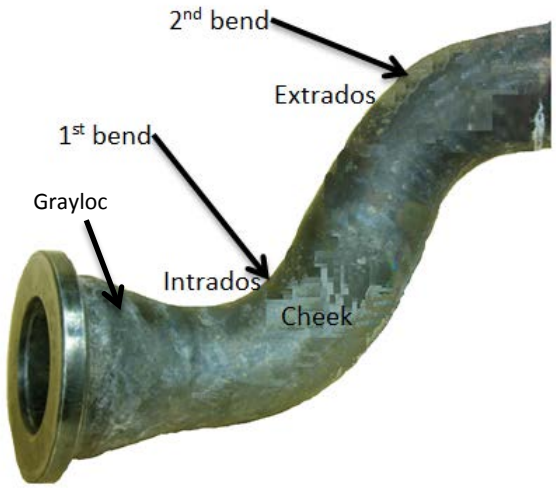

Figure 1: A feeder removed from a nuclear plant.

Ultrasonic technology has been widely used to measure wall thickness for nuclear pipes. The ultrasonic scanning systems used in CANDU industry typically consists of 6 or 14 probes, arranged within an array or bracelet. This study uses only the 14-probes scan data. Unlike the 6-probe system that can only scan along the circumferential direction of a pipe, the 14-probe technology allows scanning along the axial direction. To cover the full circumference, a feeder pipe is typically scanned four runs, each covering one of the four zones mentioned above. For 2.5-inch feeder pipes, there exists significant overlapped scan region between every two neighboring runs.

To construct a full wall thickness profile from the scan data, two challenges arise: aligning the different ultrasonic scans, and interpreting missing data present in each scan. Clearly, the presence of missing data greatly affects the first task. Missing data are caused by lose of contact between the probe and wall surface. Figure 2 depicts graphically the extent of missing data due to lose of contact. Except for intrados, each patch involves significant empty areas indicating the scan data are missing. On the other hand, the scan spacing of the data in the axial direction is 1 mm, whereas the circumferential spacing (i.e., the distance between two neighboring probes) is roughly 6 mm. This means that the best alignment accuracy in circumferential direction is 6 mm. However, inspection experience has consistently indicated that the scanning positions at the overlapping zones do not necessarily match. Therefore, accurate identification of the offset requires a finer grid of data, for example, 1 mm x 1 mm. Clearly, estimating the wall thickness at the unscanned locations is the same as estimating the missing data at the loose contact positions. Therefore, both can be called the missing data problem.

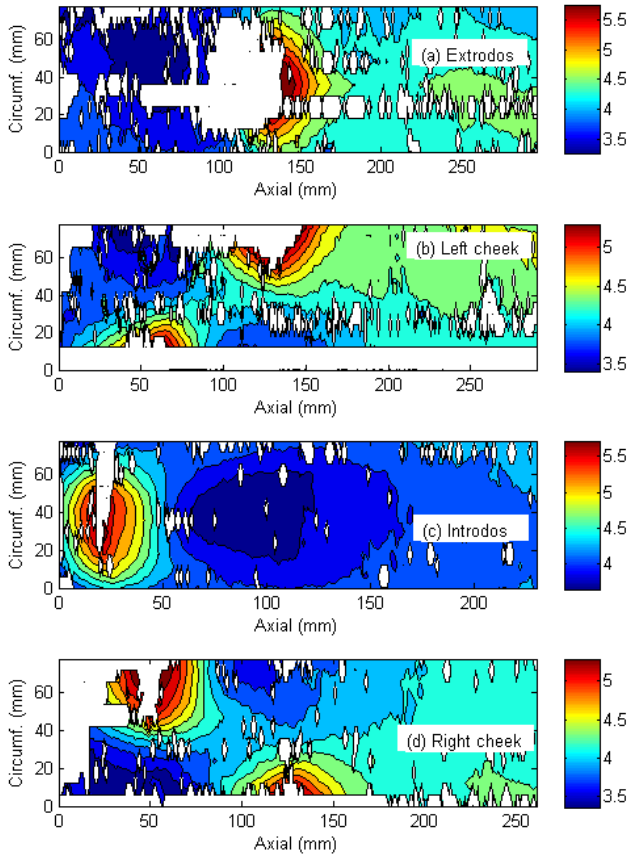

Figure 2: Ultrasonic scan plots showing missing data.

Meanwhile, although a number of inspections have been made along the service life of the pipes, with each inspection outage generating a snapshot of the random field, predicting the time trend of wall thinning remains a third and yet more challenging issue. Although this paper focuses on the spatial modeling of inspection data at one outage, the aligning methodology developed herein for different scan patches can be equally applied to the alignment of the scan data at the same scan patch from two inspections.

This study focuses on the construction of the wall thickness profile based on the ultrasonic scan data in one inspection, whereas the evolution of the thickness profile will be studied later. The paper employs a moving-window kriging technique to estimate the missing data, and a two-dimensional cross correlation function to find the matching points of any two neighboring patches.

The paper is organized as follow. The basic concepts of random fields and kriging techniques are introduced as the background in Section 2. Section 3 describes the overall methodology used to develop the wall thickness profile. The case study is presented in Section 4. The paper is concluded with major findings and recommendations in Section 5.

2. RANDOM FIELD AND KRIGING

2.1. Random Field and Semivariogram Function

A random or stochastic field, say $W(x)$ is a function whose values are random variables in space (Vanmarcke 1983). Random fields may also exist in two or three dimensional space, that is $W(x,y)$ or $W(x,y,z)$ respectively. Without loss of generality, the spatial index is denoted hereafter by s, which can be a vector. A random field may include further time as its fourth dimension, i.e., $W(s,t)$ In this case, a spatiotemporal random field presents.

Although stationarity and homogeneity are often used interchangeably to characterize some sort of stability of fluctuation, we use stationarity to describe time-related stability, and homogeneity for spatially related stability. Mathematically speaking, stationarity and homogeneity are dealt with in the same way.

Wall thinning in nuclear pipes is a nonstationary nonhomogeneous random field. It is nonstationary because there is a relatively clear trend of wall thinning along time. It is also nonhomogeneous because evidences support that the wall thinning tends to localize at the bends and grayloc positions, as mentioned previously in Section 1. This study does not consider nonstationarity and temporal variation because all the data available are measurements of wall thicknesses at one inspection outage.

There are strong homogeneity and weak homogeneity. In engineering analysis, often the weak or second-order homogeneity is used. A second-order homogeneous random field has a constant mean and standard deviation function. That is, $\mu(s) = \mu$ and $\sigma(s) = \sigma$. Moreover, the autocovariance function is independent of absolute position and it is only the function of the relative distance, or spatial lag, i.e., $C(s,h) = C(h)$, where h represents the spatial lag, which, again, can be a vector, depending on the context.

Semivariogram function is a very important concept in spatial statistics. Usually denoted by $\gamma(h)$, it is defined as

$$2\gamma(h) = var[W(s+h) - W(s)] \qquad (1)$$

The whole term $2\gamma(h)$ is called variogram function. For a homogeneous random field, it is readily shown that $2\gamma(h) = \sigma^2\big(1-\rho(h)\big) = \sigma^2 - C(h)$, where $\rho(h)$ is the auto-correlation function ranging from -1 to +1. Since $\rho(0) = 1$, theoretically $\gamma(h)$ equals 0 at $h = 0$, although it can be found nonzero in statistical analysis. In this case, the semivariogram is said to have a nugget effect, which is caused by measurement errors. In spatial statistics, σ^2 is also called the sill of the variogram function.

A great variety of theoretical semivariogram models are available, for example, linear, spherical, exponential, power, Gaussian, and sine-wave. For more details of these models, refer to Cressie (1993). Among them, the most

noted ones are the exponential and Gaussian models shown below:

$$\text{Exponential: } \gamma(h) = s(1 - e^{-3h/\theta}) \quad (2)$$

$$\text{Gaussian: } \gamma(h) = s\left(1 - e^{-3(h/\theta)^2}\right) \quad (3)$$

where s is the sill and θ the correlation length. Note that the correlation length defined here is different from those defined by, e.g., Vanmarcke (1983). Here the correlation length represents the spatial distance between two locations over which the correlation equals to 0.05. This definition is adopted for kriging purpose as observations beyond this distance becomes little significance in kriging.

Majority of analytical and statistical tools for random fields were developed for homogeneous fields. For nonhomogeneous ones, either some special purpose tools are to be invented, or the nonhomogeneous field is homogenized somehow. Several researchers have proposed methodologies in the latter line of research. Vanmarcke (1983) noted that a non-homogeneous random field can be transformed to a weakly homogeneous random field $U(x)$ with constant mean and variance of zero and one respectively by

$$U(x) = [W(x) - \mu(x)]/\sigma(x) \quad (4)$$

where $\mu(x)$ and $\sigma(x)$ are the mean and standard deviation of the random field respectively. This transformation eliminates nonhomogeneity in the first-order statistics but nonhomogeneity still exists in higher order moments. In considering spatial variation of soil properties for reliability analysis, Wu et al (2012) constructed a nonhomogeneous lognormal random field by taking the product of the homogeneous random field and a depth-dependent function. Denis and Cremoux (2002) proposed a method to divide a nonhomogeneous random field into sections with constant variability or homogeneous data using the "entropy of curves". Entropy of a spatial or time series is defined as the slope of the cumulative sum of the absolute difference. Azuri et al. (2013) accounted for spatial nonhomogeneity in the rainfall intensity by using a trend and a residual.

2.2. Kriging

Kriging is an effective tool for estimating missing or unobserved data. Pioneered by Danie Krige, a mining engineer and geostatistician, kriging is basically a prediction method that involves a linear combination or weighted average of neighboring measurements. The ordinary kriging predictor belongs to a class of best linear unbiased predictor or estimator (Isaaks and Srivastava 1989; Stein 1999). This is because the weights in ordinary kriging are usually determined so as to minimize the variance of the estimator while maintaining the estimator's unbiasedness. The kriging predictor $\widehat{W}(s_0)$ is expressed as

$$\widehat{W}(s_0) = \sum_{i=1}^{n} \lambda_i W(s_i) \quad (5)$$

where λ_i are kriging weights, s_0 is the location of the point where an estimate is required and s_i are the locations with observed attributes or values. The unbiasedness condition requires

$$E\{\widehat{W}(s_0) - W(s_0)\} = 0 \quad (6)$$

where $W(s_0)$ represents the true value of the random field at position s_0 ; whereas the minimum variance dictates the determination of the weights λ_i's so that

$$\sigma_E^2 = min_{\lambda_i}\, var\{\widehat{W}(s_0) - W(s_0)\} \quad (7)$$

For homogeneous random field, an ordinary kriging with weights λ_i sum to 1 can be formulated. In this case, it can be readily shown that the optimal weights can be calculated by using the following equation:

$$\boldsymbol{\lambda} = \boldsymbol{\Gamma}^{-1}\left(\boldsymbol{\gamma_0} - \frac{\mathbf{1}'\boldsymbol{\Gamma}^{-1}\boldsymbol{\gamma_0}}{\mathbf{1}'\boldsymbol{\Gamma}^{-1}\mathbf{1}}\right) \quad (8)$$

where $\boldsymbol{\lambda} = (\lambda_1, \dots, \lambda_n)'$; $\boldsymbol{\Gamma} = \left[\gamma(s_i, s_j)\right]$, $i, j = 1, \dots, n$, is the semivariogram matrix for the observations; $\boldsymbol{\gamma}_0 = (\gamma(s_0, s_i))$ is the semivariogram vector, each element being the semivariogram function value for s_0 and s_i, and $\mathbf{1} = (1, \dots, 1)'$ is the unit vector of n elements. Details of derivation of Eq. (8) can be found in standard spatial statistics texts, e.g., Cressie (1993).

Advanced kriging techniques have been proposed in the literature for nonhomogeneous fields. For example, Harris et al (2010) used a moving window kriging technique with geographically weighted variograms (GWVs) to estimate attribute values in nonhomogeneous random fields. In their paper, isotropic GWVs were estimated at every location. Haas (1990) presented a kriging procedure for estimating the value of an attribute using a moving circular window centered at the points where estimates are required.

Advanced methods have been proposed to increase computational efficiency of kriging algorithms. For instance, Hartmana and Hössjerb (2007) used a Gaussian Markov random field to approximate a Gaussian field with a view to reducing the computational time and memory requirement for kriging. Liang and Kumar (2013) presented a computationally efficient method termed Markov Cube kriging to krige along time and space.

3. METHODOLOGY

To construct a full circumferential wall thinning profile, two major tasks are involved. We call them 'repairing' and 'stitching,' respectively. The repairing task refers to the estimation of the missing and unobserved data – we simply fix the 'holes' in Figure 2. For this, a moving window kriging is used to account for nonhomogeneity in the spatial data. This means that within each kriging window the random field is assumed to be homogeneous. Therefore, the size of the kriging window is an important parameter to be determined.

In this study, the kriging window size is determined based on the correlation length of the semivariogram function defined in Eq (2) or (3). Empirically, the semivariogram can be estimated as

$$\gamma(h) = \frac{1}{2N}\sum_{i=1}^{N}\{w(s_i) - w(s_{i+h})\}^2 \qquad (9)$$

where h is the distance between the pair of data, N is the number of paired data. A theoretical model is then fitted to the empirical semivariogram to obtain the correlation length. In order to account for possible anisotropy the semivariograms along axial and circumferential directions are calculated and fitted, respectively. Conventional least squares technique is used for the model fitting. The correlation lengths of the two directions are then used as the side lengths of the rectangular kriging window.

To avoid nonhomogeneity effects, the moving kriging window is centred at the location where the missing data is to be estimated. Therefore, for missing data at the boundary or corner of the patch, the kriging window becomes a half or a quarter of the regular size. However, given the relatively dense grids of the raw scan data, the shrunk window did not cause kriging efficiency issue. Within each kriging window, the raw data are used to re-estimate the semivariogram functions, which are further used in Eq. (8) to estimate the missing data. Initially, the measurements were 6 mm apart along the circumferential direction and 1 mm in the axial direction. The spacing was reduced to 1 mm apart in both directions after kriging.

After each of the patches are 'repaired,' they need to be stitched together to make a full 360° wall thickness profile along the whole pipe length. Because of measurement errors and misalignment at the initial positioning of the probes for each run of scan, the patches also involve axial alignment. Therefore, a two-dimensional cross correlation matrix of two neighboring patches is computed, and the matching point corresponds to the coordinates with the highest positive cross correlation coefficient.

A further issue after stitching is to deal with the overlapped wall thickness data at the same location. This study takes the minimum value among many solutions. The whole wall thickness profile is finally established. It can be visualized by using e.g., a contour plot.

4. CASE STUDY

The scan data were drawn from wall thickness measurements of a feeder pipe from an anonymous power generation company. The pipe

has nominal thickness of 5.54 mm and an outside diameter of 60 mm, which corresponds to a circumference of 188 mm. The scanned part of the pipe has two bends (See Figure 1 for illustration). There are four patches covering scans of the extrados, right cheek, intrados and left cheek of the pipe. Each scan was done with a 14-probe scanner with a circumferential coverage of approximately 149 degrees. There were missing data in the scans denoted by "NaN". Each observed measurement is a combination of the actual measurement and a measurement error.

4.1. Semivariograms and Kriging

The empirical semivariograms of the four patches at both axial and circumferential directions are estimated and illustrated in Figure 3. The exponential and Gaussian models are used to fit the empirical semivariograms, and the Gaussian model (Eq. 3) is found to outperform the exponential model for all eight cases. The solid lines in Figure 3 represent the fitted model. The estimated correlation lengths are listed in Table 1.

The sine wave pattern is consistently revealed in the axial semivariograms. Theoretically speaking, the sine wave usually indicates some sort of periodic pattern in the data. In this study, the axial direction undergoes two bends, and the wall thickness does show some regular pattern when entering and leaving a bend. Therefore, one does not need to worry about this. It is also interesting to see that the correlation lengths of the four patches are fairly close. This shows certain homogeneity around circumference.

By contrast, the circumferential correlation length exhibits greater variation, particularly between extrados/intrados and the cheeks. This is also reasonable, because the flow in terms of turbulence characteristics at the intrados or extrados and that at the cheeks are very different. Therefore, the wall thinning characteristics are also different.

Thus, a kriging window of 100 mm (axial) x 30 mm (circumferential) is used for the extrados and intrados. For the two cheeks, the window size is selected to be 100 mm (axial) x 78 mm (circumferential). Note that 78 mm is the scan width of every patch (14 probes with 6 mm spacing).

Table 1: Estimated correlation length for the patches

Patch	*Axial*	*Circumferential*
	θ_x (mm)	θ_y (mm)
Extrados	*96.5*	*28.4*
Left Cheek	*100.4*	*78.5*
Intrados	*89.3*	*27.9*
Right Cheek	*110.8*	*50.9*

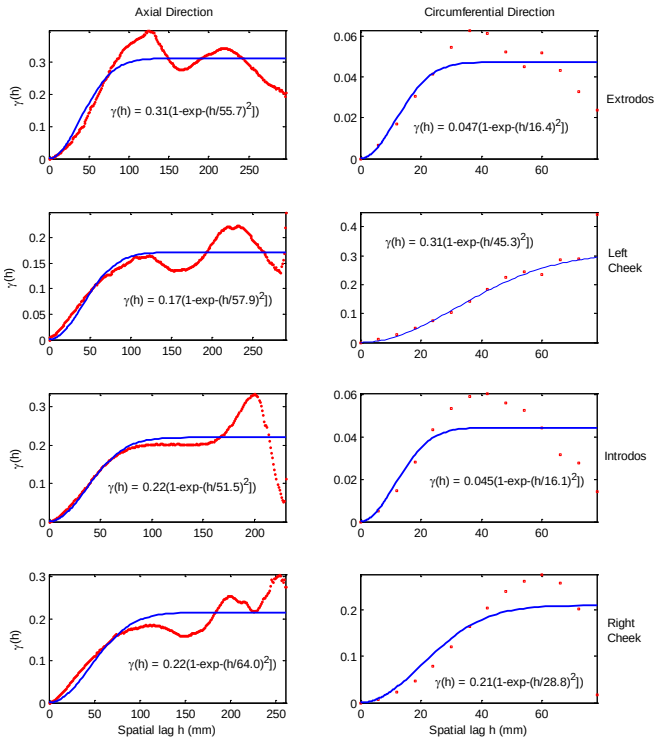

Figure 3: The empirical and fitted semivariograms.

The kriged patches are illustrated in Figure 4. While the missing data are fixed, the maximum and minimum wall thicknesses over the whole region of every patch are not changed.

4.2. Cross Correlation and Matching Points

Using the kriged random field data, the cross-correlation matrices are computed with positive and negative lags at both directions. The contour plots for all of all the four neighboring pairs are shown in Figure 5. The maximum cross

correlations and their corresponding positions (+) are illustrated as well. Clearly, for all four cases the maximum cross correlation is 0.95 or higher, indicating a good confidence of matching.

The exact offsets of the matching points are listed in Table 2. It shows that the extent of overlap in the circumferential direction varies among scans. Also, the probes were not perfectly aligned in the axial direction i.e. the scans do not start from the same position in the axial direction.

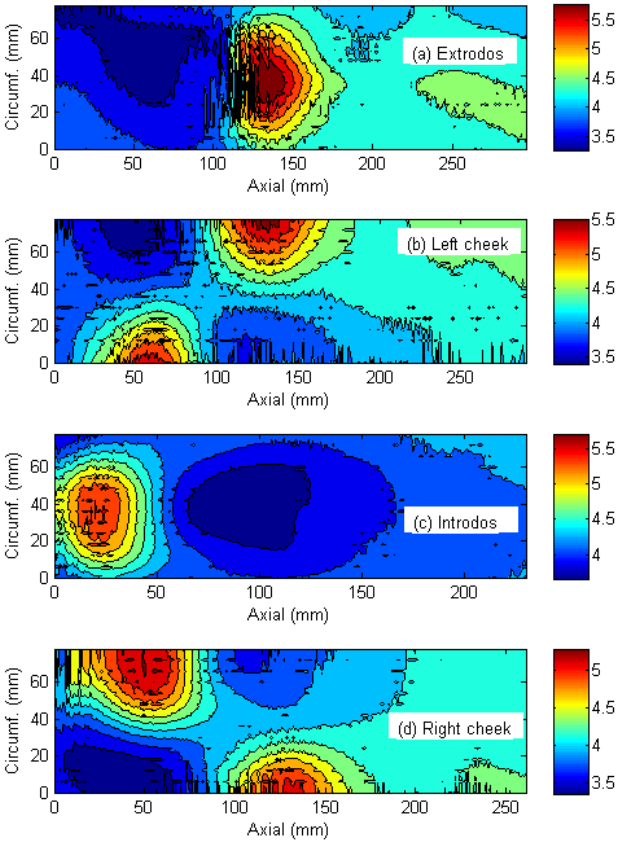

Figure 4: Random fields of the four scan patches.

Due to statistical error, the estimated offsets do not close up. However, the gap is very small. For example, the sum of the axial offset of the four patches has a net gap of 6 mm, whereas the total circumference based on the identified circumferential offsets would be 176 mm, yielding a net gap of -12 mm, in comparison with the total circumference of 188 mm. To close up, an ad hoc offset adjustment procedure was introduced in computation. The final adjustment is also shown in the table.

Table 2: Offsets of the scan patches identified by cross-correlation, with adjustment in parentheses.

	Axial (mm)	Circumf. (mm)
Ex-LC	11 (12)	-46 (-44)
LC-In	36 (30)	-42 (-42)
In-RC	-28 (-30)	-38 (-42)
RC-Ex	-13 (-12)	-50 (-48)

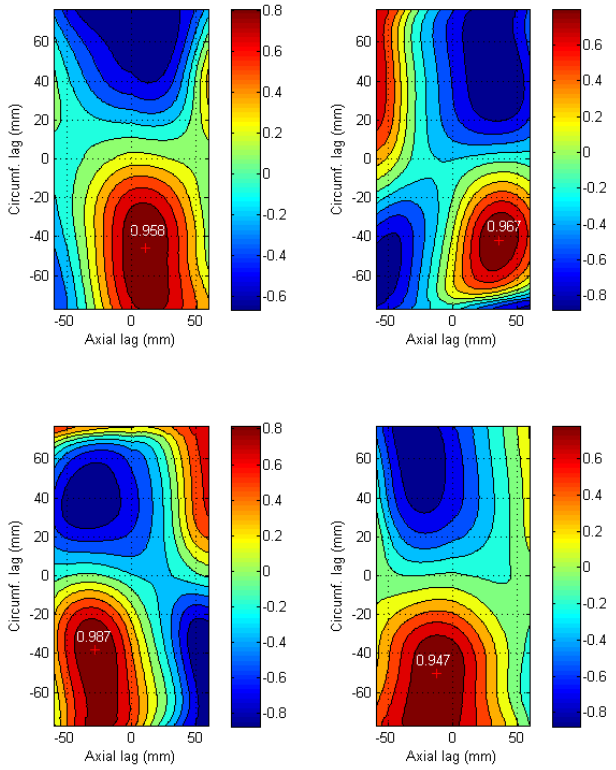

Figure 5: Cross correlation contour plots for the four pairs of scan patches.

Based on the obtained matching points, the four scan patches are stitched together to obtain a full characterization of the random field. By taking the minimum value of overlapped position, the contour plot of the combined random field is shown in Figure 6. This plot starts with extrados at the bottom, followed by right cheek and intrados, and finally the left cheek at the top. The two bends are clearly shown, one centered around 60 mm in axial

direction, and the other centered around 140 mm. Also it can be seen that the extrados at the first bend becomes intrados (thicker) at the second bend. The globally minimum wall thickness remains unchanged from the raw scan data, which is 3.269 mm.

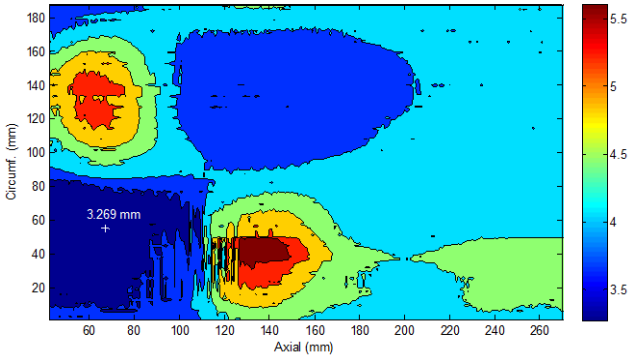

Figure 6: Contour plot of combined random field.

5. CONCLUSIONS

Wall thickness profile is a key parameter for structural integrity assessment of nuclear pipes subject to wall thinning due to FAC. This paper presents a 'repairing and stitching' technique to construct the wall thickness profile from field ultrasonic scan data. A moving-window kriging technique was used to estimate the missing and unobserved scan data. The kriged data were then used to estimate the two-dimensional cross correlation to identify the matching points of the neighboring patches for stitching purpose.

The combined random field of the wall thickness can serve as a key input for the next stage of finite element or stochastic finite element analysis for structural integrity assessment. Moreover, the 'repairing and stitching' technique also provides a useful tool for future spatiotemporal degradation modeling.

6. REFERENCES

Azuri, G., Jódar, J., Carrera, J., Gupta, H. (2013). "Stochastic simulation of nonstationary rainfall fields, accounting for seasonality and atmospheric circulation pattern evolution." *International Association for Mathematical Geosciences*, 45, 621–645.

Chung, H. (2010). "A review of CANDU feeder wall thinning." *Nuclear Eng. and Design*, 42(5).

Cressie, N. A. C. (1993). *Statistics for Spatial Data*. Revised edition. John Wiley & Sons, Hoboken, New Jersey.

Denis, A., Cremoux, F. (2002). "Using the entropy of curves to segment a time or spatial series." *Mathematical Geology*, 34(8), 899-914.

Fenton, G. and Griffiths, D. (2008). *Risk Assessment in Geotechnical Engineering*. John Wiley & Sons, Hoboken, New Jersey.

Haas, T. (1990). "Kriging and automated variogram modeling within a moving window." *Atmospheric Environment*, 24(7), 1759 – 1769.

Harris, P., Charlton, M., Fotheringham, A. (2010). "Moving window kriging with geographically weighted variograms." *Stochastic Environmental Research and Risk Assessment*, 24(8), 1193 – 1209.

Hartmana, L., Hössjerb, O. (2007). "Fast kriging of large data sets with Gaussian Markov random fields." *Computational Statistics & Data Analysis*, 52, 2331 – 2349.

Isaaks, E., Srivastava, R (1989). *Applied Geostatistics*. Oxford University Press. *New York.*

Jin, J., Awad, R. (2011). "Fitness for service assessment of degraded CANDU feeder piping-Canadian regulatory expectations." *Journal of Nuclear Engineering and Design*, 241(3):644-647.

Liang, D., Kumar, N. (2013). "Time-space Kriging to address the spatiotemporal misalignment in the large datasets." *Atmospheric Environment*, 72, 60 – 69.

Slade, J., Gendron, T. (2005). "Flow accelerated corrosion and cracking of carbon steel piping in primary water – Operating experience at the Point Lepreau Generating Station." *Proceedings of 12th Int Conf on Environmental Degradation of Materials in Nuclear Power System*, Salt Lake City, 773-784.

Stein, M. (1999). *Interpolation of Spatial Data: some theory for kriging*. Springer, New York.

Vanmarcke, E. (1983). *Random fields analysis and synthesis*. Princeton University Press. Also the revised edition, by World Scientific, 2010.

Wu, S.H., Ou, C.Y., Ching, J.Y., Juang, C.H. (2012). "Reliability-based design for basal heave stability of deep excavations in spatially varying soils." *Journal of Geotechnical and Geoenvironmental Engineering*, 138(5), 594-603.